Catalysis Science & Technology

Accepted Manuscript

ROYAL SOCIETY OF CHEMISTRY

www.rsc.org/catalysis

Optimization of the Catalytic Hydrogenation for Terebinth by a Ni-Based Catalyst

Linlin Wang, Huiqing Guo, Xiaopeng Chen*, Qingmei Chen, Xiaojie Wei, Yonghui Ding, Bixin Zhu

School of Chemistry and Chemical Engineering, Guangxi University, Key Laboratory for the Petrochemical Resources Processing and Process Intensification Technology of Guangxi, Nanning, 530004, PR China

*Corresponding author. Tel.: + 86 771 3272702; fax: + 86 771 3233718.

E-mail address: lilm@gxu.edu.cn

Optimization of the Catalytic Hydrogenation for Terebinth by a Ni-Based Catalyst

Linlin Wang, Huiqing Guo, Xiaopeng Chen*, Qingmei Chen, Xiaojie Wei, Yonghui Ding, Bixin Zhu

School of Chemistry and Chemical Engineering, Guangxi University, Key Laboratory for the Petrochemical Resources Processing and Process Intensification Technology of Guangxi, Nanning, 530004, PR China

Abstract: Cumulative amounts of waste equilibrium fluid catalytic cracking catalyst (Ecat) are generated in the petrochemical industry every year. They are contaminated by poisons heavy metal ions, and are dumped into landfills, posing the difficulties in solid waste management and resulting in heavy environmental problem as well as the resource waste. Thus, using the (Ecat) as supporter, a new non-noble metal supported Ni catalyst (Ni/Ecat) was synthesized and applied to convert terebinth, a renewable feedstock, to value-added pinane. The catalyst was characterized by SEM, XRD, FIIR and TPR. In the hydrogenation process important variables like temperature, pressure, reaction time and stirring speed have been studied by response surface methodology (RSM). The optimum reaction time, temperature, hydrogen pressure, and stirring speed were found to be 2.3 h, 110 °C, 3.2 MPa and 540 rpm, respectively, with the conversion of terebinth 98.90% and the selectivity of *cis*-pinane 94.00%. This result

clearly showed that Ni/Ecat exhibited high activity, selectivity and good stability. The Ni/Ecat can be reused 13 times with terebinth conversion of 93.73% and the selectivity of *cis*-pinane 93.60%.

Keywords: Ecat; Ni/Ecat; Terebinth; Hydrogenation; Optimization

Introduction

The fluid catalytic cracking (FCC) is the most important part in modern refinery processes.[1] While the FCC catalyst will face the deactivation phenomena because of coke and substantial deposits of heavy metal contaminants such as Ni, Fe and V.[2] Therefore, environmental pollution is the main problem for disposal of waste FCC catalyst (Ecat). The major mode of processing residual Ecat is dumped into landfills.[3-4] These residuals are stable and fast, posing the difficulties in solid waste management and result in significant environmental disturbances as well as the resource waste.

It is noted that the amount of Ecat is 6–9 metric tons/day.[5] Since Ecat consists of a crystalline zeolite Y and amorphous silica-alumina/alumina, and Ni deposited in Ecat is the active component of hydrogenation, Fe deposited in Ecat is an assistant of hydrogenation.[6] Increasing concerns of environment and the shortage of resource has result in considerable efforts being made to recover various valuable waste materials. In literature, there are many studies on the treatment of Ecat. Most of these studies are limited to using as adsorbent[7] and as an admixture in construction materials [8-9] as well as the regeneration via the method of removing heavy metals existed in Ecat.[10] In the removing heavy metals, not only toxic gases, corrosive gases and liquid acids used, but secondary pollution to the environment. Until now, no special research has referred to the reuse of these poisonous ions deposited on the Ecat, such as Ni, V, and Fe and the use of Ecat as catalyst supporter. However, in the above study, these heavy metals need to be removed, in which not only exists high energy consumption and cost but the use of liquid acids also causes the secondary pollution to the environment. Therefore, in this paper, not only Ni, the main deposition component in Ecat was

taken advantage of but Ecat was also used as catalyst carrier supported Ni (partial supplement via nickel nitrate) to prepare load-type noble metal-free catalyst by the wet impregnation technology, without the removing of heavy metals. It is well known that the catalytic hydrogenation is one kind of the most important organic chemical reactions.

Increasing crude oil prices, the impact on climate change and the decreasing oil reserves will prompt increasingly concerned about the use of biomass resources in the near future. Therefore, the production of value added chemicals and materials from renewable resources play a more and more dominate role in the future chemical industry. Terebinth is a well-known essential oil obtained from various species coniferous trees. It is mainly composed of bicyclic monoterpenes, α-pinene and β-pinene, thus, the main hydrogenation product of terebinth is pinane.[11] The above transformation process is an important process in the perfumery, food and pharmaceutical[12] because pinane is versatile feedstock or synthetic intermediates for series of chemicals. Generally, both *cis*- and *trans*-pinane are the products of the hydrogenation of terebinth. However, due to the present of steric hindrance, pose the hydrogenation process towards the formation of *cis*-pinane.[13] The main catalysts for hydrogenation of pinenes to pinane are noble metals such as Pd/C, Pt/C and Ru/C,[14-17] which are expensive, among which Pd/C catalyst is already widely used in the industrial production of pinane. However, the manufacturing cost is getting higher with the increasing price of Pd. Hence, in recent years interests are growing in the use of alternative noble metal-free catalyst.

In this study the following objectives were undertaken (i) to prepare and characterization the Ni/Ecat catalyst, (ii) to optimize the maximum conversion of terebinth and the best selectivity of *cis*-pinane using response surface methodology and (iii) to study the effect of temperature, hydrogen pressure, reaction time and stirring speed on the conversion of terebinth and the selectivity of *cis*-pinane.

Materials and methods

Material

The Ecat was provided by one of the oil refineries in Guangxi, China and is composed mainly of SiO_2 and Al_2O_3. The catalysts had a powder shape; its surface area and pore volume were 96.12 m^2/g and 0.19 cm^3/g, respectively. The partial chemical elements of the spent catalyst included (wt%) O: 50.17%; Al: 24.89; Si: 17.72; Ni: 3.68; Fe: 2.01%. The Ni/Ecat was prepared by wet impregnation[18-20] of an aqueous solution of nickel nitrate. Specifically, Ecat support was pretreated by roasting in order to clear up the coke deposited on Ecat surface. Then, the impregnation was conducted at 30 °C for 2 h. After impregnation, the samples were dried at 110 °C for 6 h, calcined at 500 °C for 3 h, and finally reduced at 500 °C in hydrogen flow for 2 h. The nickel load was maintained constant at 15 wt%.

Terebinth was provided by a chemical plant (Guangxi Ningming Pine Chemicals Ltd.) in Guangxi province, China. The composition of terebinth was: α-pinene, 91.9%, β-pinene, 5.6%, longifolene, 2.4%. Nickel nitrate hexahydrate ($Ni(NO_3)_2 \cdot 6H_2O$), hydrogen (purity > 99.0%) and nitrogen (purity > 99.0%) were purchased from Guangdong Guanghua equipment Co., Ltd., China and used as received.

Catalyst characterization

SEM images of the catalysts and SEM-EDS analysis were taken on a Hitachi SU-8000 scanning electron microscope, using secondary electrons to form the images. Before testing, in order to ensure sufficient conductivity the gold was sputtered onto the catalysts.

The structures of the Ecat and Ni/Ecat were characterized by X-ray diffraction (XRD) technique on a Rigaku Smartlab X-ray diffractometer. Cu, K_α radiation was used at 40 kV and 25 mA in a scanning range of 10–80° (2θ) at a rate of 8°/min.

Fourier transform infrared (FT-IR) spectra were recorded on a United States NICOLET 6700 Fourier transform infrared spectrometer by KBr pellet technique. The spectra were recorded at 2.0 cm^{-1} resolution in the scanning range 4000–400 cm^{-1} to analyze the functional groups.

A FINESORB 3010C adsorption system equipped with a TCD detector was taken to carry out H_2–TPR analysis. In a typical method, about 500 mg of catalyst sample was pretreated in He flow (40 mL/min) at 300 °C for 2 hours. After cooling down to room temperature, the adsorption experiment was heated from room temperature up to 1000 °C (heating ramp of 15 K/min) in a N_2 flow and the desorption of H_2.

Catalytic activity measurement

The hydrogenation of terebinth was carried out on a stainless steel autoclave (2-L), with a double-tiered paddle agitator. In a typical run, 700 g of the terebinth and a specified quantity of the catalyst were loaded into the reactor. The reactor was purged with H_2 (99.99%; Guangxi guoxin gas research Co., Ltd.) to given reaction

pressure. The mixture of the terebinth and the catalyst was heated up to reaction temperature with desired agitation speed and reaction time.

After the reaction, the liquid phase products were separated from the catalyst by filtration. These products were analyzed via a gas chromatography instrument (7820A) equipped with a flame ionization detector (FID). The components were separated on a DB-5 column of 30 m length, 0.32 mm internal diameter and 0.25 μm film thickness. The oven temperature was programmed at 60 °C for 2 min and increased to 62 °C by 0.2 °C/min and from 62 °C to 170 °C at 15 °C/min, and finally held at 170 °C for 2 min. The injector and detector temperatures were both 250 °C. Nitrogen was used as the carrier gas at a flow rate of 45 mL/min.[21]

GC–MS analysis was performed using Agilent gas chromatography (6850 GC) with a DB-5MS column (30.0 m × 320 μm × 0.25 μm) and a quadrupole mass filter equipped 5975 mass selective detector (MSD). A 0.2 μL injection volume was used with an injector temperature of 250 °C. The temperature program began at 60 °C and increased to 80 °C at a rate of 1 °C/min, after which the temperature increased at a rate of 10 °C/min to 160 °C, and finally increased to 250 °C, where it was held for 2 min. The mass spectrometer source temperature and the electron energy were 250 °C and 70 eV, respectively.

Experimental design, statistical analysis and optimization

A three level, four variable Box–Behnken factorial designs (BBD) was performed using the statistical software (Design-Expert 7.0) to determine the best conversion of terebinth and the selectivity of *cis*-pinane.[22-23] Three variables

considered for this research was designated by -1 (minimum), 0 (medium), +1 (maximum), and the proper ranges of three variables were determined on the basis of single-factor experiment. The ranges and the levels of the variables investigated in this study are given in Table 1. The most suitable array for this experiment is $L_{27,}$ therefore, the factorial design consists of 27 experimental points, based on four independent variables at each of the three levels. The BBD shown in Table 2 presents the experimental conditions and their responses.

In order to correlate the dependent and independent variables, the quadratic polynomial equation was used for fitting both the conversion of terebinth and the selectivity of *cis*-pinane:

$$Y = b_0 + b_1A + b_2B + b_3C + b_4D - b_{12}AB + b_3AC - b_{14}AD + b_{23}BC - b_{24}BD - b_{34}CD - b_1^2A^2 - b_2^2B^2 - b_3^2C^2 - b_4^2D^2 \quad (1)$$

where Y is a predicted response variable of the combination of each factor lever; b_i is the regression coefficients of independent variables; b_{ii} is the regression coefficients for squared terms; b_{ik} is the regression coefficients for interaction, and A, B, C and D are coded experimental levels of the variables.

Result and discussion

Characterization

Fig. 1a shows the scanning electron micrograph (SEM) of Ecat, in which a coarse, porous, and spherical structure was observed at Ecat. It indicates that Ecat has a large surface area, and thus, it is feasible to take it as the catalyst supporter. Fig. 1b presents the image of NiO/Ecat, appearing amount of plate-like particles. These grains

could be NiO, which distributed on the surface of the catalyst and the inter layer at a crystalline structure homogeneously. The SEM results indicate that the annealed NiO/Ecat catalyst with a better activity, hence there will be excellent result of hydrogenation of the terebinth. The nickel load was 13.8 wt% identified via SEM-EDS.

The XRD patterns of Ecat and Ni/Ecat (store in the air for period of time) are shown in Fig. 2. The ZSM-5 zeolite ($Na_{2.2}Al_2Si_{91}O_{186.1}$, PDF-00-43-0322) and Y zeolite ($Na_{48.8}Al_{48.8}Si_{143.2}O_{284}$, PDF-00-081-2466) and amorphous (glassy) aluminosilicate phases were observed at Ecat, which are identifiable by the Powder Database File. Thus, it is feasible to take it as the catalyst supporter, which agrees with the result of SEM. Diffraction peaks at 42.5°, 52.3° and 76.6°, corresponding to Ni(111), Ni(200) and Ni(220) plans of the centered cubic nickel (PDF-04-0850), respectively, were appeared at Ni/Ecat. This indicates that the Ni existed in Ni/Ecat is in a completely crystalline form. There are no peaks of NiO, which shows that the catalytic performace of the Ni/Ecat is stable. Therefore, the time of the reuse of Ni/Ecat may be long.

As shown in Fig. 3, the peak of Ecat is similar to zeolite Y.[24] The band at 1080-1090 cm^{-1} was assigned to the silicon (Al) tetrahedra (TO_4) antisymmetric stretching vibration, nearing the 780 cm^{-1} was the symmetric stretching vibration of TO_4 activity peaks, TO (T = Si or Al) bending vibration peaks change in 442-450 cm^{-1}. Broad absorption peak near 3480-3590 cm^{-1} was the stretched vibration of physically adsorbed water, while, 1640 cm^{-1} absorption peak was the bending vibration of the

physically adsorbed water. Compare the Ecat to the Ni/Ecat, the absorption band for the Si–H stretching vibration has been observed at 2350 cm^{-1}. There was no absorption at 980 cm^{-1} of Si-O(H)-Ni at NiO/Ecat, which illustrates that no valent bond between the metal and the support, therefore, Ni/Ecat is easy obtained via the reduction of NiO/Ecat.

Fig. 4 presents the results of the H_2-TPR analysis performed over the NiO/Ecat. The TPR spectra show two peaks, one was a low H_2 consumption peak centered in the temperature range of 300–600 °C and another was a high temperature peak approximately at 855 °C. According to the literature[25-26], the peak in the 300–600 °C temperature range was assigned to the reduction of Ni^{2+} in the NiO phase, its complexity may be ascribed to the presence of different NiO species.[27] The high intensity of the peaks indicates that the amount of NiO is large and the low temperature peak explains the weak interaction of the metal and the support, and thus, it is easy to be reduction. So, large amount of Ni/Ecat can be obtained. This is agreeing with the result of FIIR.

In order to evaluate the activity of Ecat, a blank experiment on Ecat and an experiment with fresh FCC were run at 120 °C, 4 MPa, and 2 h of reaction time, and the result indicating that the selectivity of *cis*-*trans* pinane were 82.50% and 67.70%, the yield of *cis*-pinane were 10.48% and 0.81%, respectively. The experiment was also conducted over the amount of 5% Raney nickel catalyst (commercial 60%), and the selectivity of *cis*-*trans* pinane was 92.70, the yield of *cis*-pinane was 48.20%.

Catalyst usage and reuse

While maintaining the same reaction conditions (temperature 120 °C, pressure 4.0 MPa, reaction time 2 h and stirring speed 500 rpm) we explored the relations between the catalyst usage and the conversion and the relations between the catalyst usage and selectivity, which are shown in Fig. 5a. The conversion of terebinth increased with the dosage of catalyst at 2-4% sharply, which existing a slight change when at prolonged raise of the dosage of 5 to 6%. However, the dosage of catalyst had no effect on the selectivity of *cis*-pinane. Therefore, the most appropriate dosage of catalyst was 5%.

The possibility of reusing the catalyst was established at 110 °C, 4.0 MPa of H_2 pressure and at 600 rpm for 2.0 h, the catalyst dosage was 5%. The testing results are presented in Fig. 5b. The specific operation was performed as follows: In a typical run, 700 g of terebinth and 35 g of catalyst were put into the autoclave. After a typical run, the supernatant clear product mixture was removed from the reactor. Finally, the fresh charge of terebinth was loaded to the catalyst residue in the reactor and the subsequent run was continued under the same conditions. As can be seen from Fig 5b, after 13 times of reaction, the terebinth conversion of 93.73% was obtained, which is about 94.86% of the original activity. The selectivity of *cis*-pinane ranges from 93.60 to 94.20%. These results indicate that the structure of the catalyst was stable. In order to investigate the features of the deactivation, the used catalysts will be characterized in future studies.

Model fitting and adequacy checking

In order to verify the main effects and the interaction effects of each other on the

conversion of terebinth and the selectivity of *cis*-pinane, the analysis were carried out based on the hydrogenation experiments. The primarily effects factors is decided via analysis of variance (ANOVA). The results of ANOVA are presented in Table 3.

Result for the conversion of terebinth

The result for turebinth conversion according to the experimental design is presented in Table 3a. The larger the magnitude of the *F*-value and smaller the *P*-value, the more significant is the corresponding coefficient.[28] It can be seen from the Table 3a that the model *F*-value of 14.45 implies that the model is significant, and the *P*-values less than 0.0001 (95% confidence intervals) indicate that the model terms of the conversion of terebinth are significant. These results imply that all the independent variables (*A*, *B*, *C*, *D*) and three quadratic terms (A^2, B^2, C^2) significantly affect the conversion of terebinth, and there is significant interaction between temperature (*B*) and stirring speed (*D*) ($P < 0.05$). Based on the ANOVA results, Eq. (4) was obtained and further used to fit the experimental data of the conversion of terebinth.

$$Y_1 = 93.31 + 11.61A + 18.58B + 22.42C + 7.11D - 5.79AB + 2.31AC - 0.79AD + 2.81BC - 9.79\,BD - 6.07\,CD - 13.33A^2 - 12.28B^2 - 20.64C^2 - 3.23D^2 \quad (2)$$

where *A, B, C* , *D* and Y_1 are the pressure (MPa), temperature (°C), reaction time (h), stirring speed (rpm) and the conversion of terebinth, respectively.

The determination coefficient R^2 of the effect on the conversion of terebinth is $R_1^2 = 0.944$ based on the reliability analysis for the regression equation. The result indicates that more than 94% of the experimental data can be used to explain the

influence on the conversion of terebinth and also mean that only less than 6% of the total variation does not fit the model. These predicted vs. actual values of the conversion of terebinth are shown in Fig. 6a. These results clearly reveal that a well correlation between the experimental data and the predicted values because of the clustering of the points around the diagonal line, confirming the validity of the model. These results prove that an experimental design of the Box-Behnken model can be effectively applied for optimization of the conversion of terebinth.

The Pareto analysis provides more significant information to interpret the importance of the factors and interactions, which is conducted according to the following relation[28-29]:

$$P_i = \left(\frac{b_i^2}{\sum b_i^2} \right) \times 100 (i \neq 0) \quad (3)$$

Fig. 6b shows the Pareto graphic analysis of the conversion of terebinth. The contributions of the principal effects (*A, B, C* and *D*) on the percentage of the conversion of terebinth are 6.81%, 17.45%, 25.41% and 2.56%, respectively. The contributions of the interaction effects (*AB*, *AC*, *AD*, *BC*, *BD* and *CD*) on the percentage of the conversion of terebinth are the following: 1.69%, 0.27%, 0.03%, 0.40%, 4.85% and 1.86% respectively. Thus, the effect of *AC*, *AD* and *BC* can be negligible because the response less than 1%. The contributions of the quadratic parameters (A^2, B^2, C^2 and D^2) on the percentage of the conversion of terebinth are 8.98%, 7.62%, 21.54% and 0.53%, respectively. These results suggest that among the variables, *B* (17.45%) (temperature), *C* (25.41%) (reaction time) and squared effect of reaction time (21.54%) (C^2) produce the largest effect on the conversion of terebinth.

Result for the selectivity of cis-pinane

The result of the selectivity of *cis*-pinane is presented in Table 3b. *F*-value of 18.61 and a *P*-value ($P<0.0001$) indicate that the model is also significant. These results demonstrated that all the independent variables (*B*, *C*) and three quadratic terms (C^2, D^2) significantly affect the selectivity of *cis*-pinane, and there is significant interaction between reaction time (*C*) and stirring speed (*D*) ($P < 0.05$).

Based on the ANOVA results, Eq. (6) was obtained and further used to fit the experimental data of the selectivity of *cis*-pinane.

$$Y_2 = 90.55 + 0.32A - 1.76B + 1.75C + 0.1D + 0.42AB - 0.094AC + 0.056AD - 0.24BC - 0.073BD - 1.07CD - 0.13A^2 + 0.29B^2 - 1.38C^2 + 0.69D^2 \quad (4)$$

where *A, B, C* , *D* and Y_2 are the pressure (MPa), temperature (°C), reaction time (h), stirring speed (rpm) and the selectivity of *cis*-pinane, respectively.

The determination coefficient R^2 of the effect on the selectivity of *cis*-pinane is $R_2^2 = 0.956$ implies that about 95.6% of the variations for the selectivity of *cis*-pinane are explained by the independent variables and this also mean that the model does not explain only about 5% of the total variation. The predicted vs. actual values of the selectivity of *cis*-pinane are shown in Fig. 7a. These results confirm that the experimental data are in good agreement with the predicted values, due to the experimental data near to the straight line, indicating a satisfactory correlation between these values. These results illustrate that an experimental design of the Box-Behnken model can be effectively applied for optimization of the selectivity of *cis*-pinane.

Fig. 7b shows the Pareto graphic analysis of the selectivity of *cis*-pinane. .The contributions of the principal effects (*A, B, C* and *D*) on the percentage of the selectivity of *cis*-pinane are 1.01%, 30.52%, 30.17% and 0.10%, respectively. The contributions of the interaction effects (*AB*, *AC*, *AD*, *BC*, *BD* and *CD*) on the percentage of the selectivity of *cis*-pinane are the following: 1.74%, 0.09%, 0.03%, 0.57%, 0.05% and 11.28% respectively. Thus, the effect of *AC*, *AD*, *BC* and *BD* can be negligible because the response less than 1%. The contributions of the quadratic parameters (A^2, B^2, C^2 and D^2) on the percentage of the selectivity of *cis*-pinane are 0.17%, 0.83%, 18.76% and 4.69%, respectively. The results suggest that among the variables, B (17.45%) (temperature), C (30.17%) (reaction time) and squared effect of reaction time (18.76%) (C^2) produce the largest effect on the selectivity of *cis*-pinane.

Effect of various factors

Effect of the parameters on the conversion of terebinth

Fig. 8a represents the effect of pressure and temperature on the conversion of terebinth under the predefined conditions given by model. It is clear that the pressure and temperature had positive impact on the conversion of terebinth, the conversion of terebinth increased rapidly with increasing of pressure and temperature at fixed reaction time of 2 h and stirring speed of 600 rpm. Such as, the conversion of terebinth is 32% at 100 °C and 2 MPa, however, the conversion of terebinth reached to the maximum 97.61% at 120 °C and 4 MPa.

The conversion of terebinth for the temperature of 110 °C with stirring speed at 600 rpm obtained as a function of the pressure and reaction time is depicted in Fig. 8b.

As it is clear from the figure, the conversion of terebinth reached to the highest value at 99.5% when the reaction time was about 2.5 h at 3 MPa. With the farther increasing of reaction time, the conversion of terebinth had a slight decrease.

Fig. 8c illustrates the effect of the pressure and stirring speed upon the conversion of terebinth for the temperature of 110 °C and reaction time at 2 h. As can be understood from Fig. 8c, the changes of the conversion of trerbinth increased with stirring speed from 58 to 77% at 2 MPa.

Fig. 8d presents the response surface and contour plots as an estimate of the conversion of terebinth as a function of two variables of the reaction time and temperature (pressure = 3 MPa; stirring speed = 600 rpm). As is obvious from Fig. 8d, the conversion of terebinth increased with increase in reaction time range of 1 to 2.5 h and reached up to the highest 65.2% after 2.5 h at 100 °C.

Fig. 8e displays the 2D and 3D plots for the conversion of terebinth as a function of the stirring speed and temperature (at a fixed pressure of 3 MPa and reaction time of 2 h). As is clear from the response surface and contour plots, the conversion of terebinth reached to high values (> 90%) after about 113 °C and the stirring speed within the specified range did not have a significant impact on color removals.

Fig. 8f shows the response surface and contour plots for the conversion of terebinth as a function of the reaction time and stirring speed for the temperature 110 °C and pressure 3 MPa. As can be seen from Fig. 8f, the high value (> 90%) of conversion of terebinth occurred when reaction time was about at 2 h under all stirring speed.

Effect of the parameters on the selectivity of *cis*-pinane

Fig. 9a represents the effect of pressure and temperature on the selectivity of *cis*-pinane under the predefined conditions given by model. It is clear that the temperature had negative impact on the selectivity of *cis*-pinane, the selectivity of *cis*-pinane decreased rapidly with increasing of temperature at fixed reaction time of 2 h and stirring speed of 600 rpm. Such as, the selectivity of *cis*-pinane is 92.02% at 100 ℃, however, the selectivity of *cis*-pinane drop down to the minimum 88.2% at 120 ℃. The change of the selectivity of *cis*-pinane with increase of pressure was neliglble.

The selectivity of *cis*-pinane for the temperature of 110 ℃ with stirring speed at 600 rpm obtained as a function of the pressure and reaction time was depicted in Fig. 9b. As it is clear from the figure, the selectivity of *cis*-pinane reached to the highest value at 91.06% when the reaction time was about 3 h and 4 MPa.

Fig. 9c illustrates the effect of the pressure and stirring speed upon the selectivity of *cis*-pinane for the temperature of 110 ℃ and reaction time at 2 h. As can be understood from Fig. 9c, the change of the selectivity of *cis*-pinane with increase of stirring speed was negligible.

Fig. 9d presents the response surface and contour plots as an estimate of the selectivity of *cis*-pinane as a function of two variables of the reaction time and temperature (pressure = 3 MPa; stirring speed = 600 rpm). As is obvious from Fig. 9d, the selectivity of *cis*-pinane increased with increase in reaction time and reached up to 90% after 2 h when the temperature less than 110 ℃.

Fig. 9e displays the 2D and 3D plots for the selectivity of *cis*-pinane as a function of the stirring speed and temperature (at a fixed pressure of 3 MPa and reaction time of 2 h). As is clear from the response surface and contour plots, the selectivity of *cis*-pinane drop to low values (< 90%) after about 115 °C and the stirring speed within the specified range did not have a significant impact on color removals.

Fig. 9f shows the response surface and contour plots for the selectivity of *cis*-pinane as a function of of the reaction time and stirring speed for the temperature 110 °C and pressure 3 MPa. As can be seen from Fig. 9f, the highest the selectivity of *cis*-pinane occurred when reaction time was about at 2.5 h, and the stirring speed has no significantly effect on the selectivity of *cis*-pinane at this time.

Optimization of response

The study was taken with the aim of achieving the desired surface roughness of the optimal cutting parameters. The results from RSM using the numerical optimization are tabulated in Table 4. The results in Table 5 pertain to the reaction at the optimized reaction condition after three parallel experiments to compare with the modeling results. The condition based on the conversion of terebinth was the reaction time = 2.3 h, temperature = 110 °C, hydrogen pressure = 3.2 MPa, and stirring speed = 540 rpm. Under the above conditions, the terebinth conversion and *cis*-pinane selectivity reached up to 98.90 and 94.00%, respectively. The % errors between the predicted and experimental results for optimization of terebinth conversion and *cis*-pinane selectivity are 1.0 and 3.3%, respectively. This condition was defined as

group a. Another condition based on the selectivity of *cis*-pinane was reaction time = 2.6 h, temperature = 101 °C, hydrogen pressure = 2.7 MPa, and stirring speed = 500 rpm, which is defined as group b, and the terebinth conversion and *cis*-pinane selectivity are 52.40 and 94.40%, respectively. The % errors between the predicted and experimental results for optimization of terebinth conversion and *cis*-pinane selectivity are 2.6 and 0.1%, respectively. The discrepancies between the predicted and experimental results may be caused the characteristic of the catalysts, which have not been considered by the statistical model. Nevertheless, the differences are within the acceptable limit.

At group a, the observed value of terebinth conversion reached the highest 98.90%, and the *cis*-pinane selectivity reached 94.00% which is near to the highest 94.40% in group b. However, at group b, the *cis*-pinane selectivity reached highest 94.40%, but the terebinth conversion 52.40% is far from the highest 98.90% in group a. Therefore, the most optimal condition is group a: reaction time 2.3 h, temperature 110 °C, hydrogen pressure 3.2 MPa, and stirring speed 540 rpm with the conversion of terebinth 98.90% and the selectivity of *cis*-pinane 94.00%. This study clearly showed that Ni/Ecat exhibited high activity, selectivity and good stability, which is resulted by the structure of the catalyst as distributed on the surface of the catalyst homogeneously and with stable performance described by SEM and XRD. These results also demonstrate that the change of *cis*-pinane selectiviy is not sensitive to the temperature, but terebinth conversion is affected by temperature significantly.

The characterizations of FIIR and TPR indicate that the Ni/Ecat can be obtained

via the reduction of NiO/Ecat easily, and the SEM and XRD demonstrate that the catalyst has better activity and stable structure. As better activity the hydrogenation achieved high conversion of terebinth and good selectivity of *cis*-pinane 94.00%. The stable structure of Ni/Ecat result in the terebinth conversion and the selectivity of *cis*-pinane of 93.70 and 93.60%, respectively after 13 times of reaction.

Conclusion

It has been shown that the conversion of renewable biomass to useful chemicals over Ni/Ecat is a feasible process. The dosage and reuse of Ni/Ecat were 5% and 13 times, respectively. In the RSM optimization process, an empirical relationship of the conversion of terebinth and the selectivity of *cis*-pinane between the response and independent variables were studied and expressed by the quadratic model of equation. Both the proposed quadratic models fit well with the experimental data, with correlation coefficients (R^2) of terebinth conversion and *cis*-pinane selectivity 0.940 and 0.956, respectively. The Pareto graphic analysis suggested that among the variables, temperature, reaction time and squared effect of reaction time produce the largest effect on the conversion of terebinth; temperature, reaction time and squared effect of reaction time produce the largest effect on the selectivity of *cis*-pinane. The optimum values of the reaction time, temperature, hydrogen pressure, and stirring speed were achieved as 2.3 h, 110 °C, 3.2 MPa and 540 rpm, respectively, with the conversion of terbinth 98.90% and the selectivity of *cis*-pinane 94.0%. The characterization techniques of SEM, XRD, FIIR and TPR combing with the result of processing optimization indicating that the Ni/Ecat have great effects on the

hydrogenation of terebinth. Therefore, the approach can be regarded useful for the optimization of the hydrogenation of terebinth over Ni/Ecat based on experimentally and statistically in this study.

Acknowledgments

We gratefully acknowledge the financial support received by the National Natural Science Foundation of China (Grant Nos. 31060102), the Guangxi Natural Science Foundation (Grant Nos. 2013GXNSFAA0190507 and 2014GXNSFDA118010), and the Key Laboratory of Petrochemical Resource Processing and Process Intensification Technology.

References

1 J. Kumar, K. R Gota and B. Modher, *APCBEE Procedia* 2014, ***9***, 159–164.
2 J. S. Yoo, *Catal. Today* **1998**, *44*, 27–46.
3 M. Marafi and A. Stanislaus, Resour. *Conserv. Recycl*., 2008, ***52,*** 859–873.
4 K. Al-Jabri, M. Baawain, R. Taha, Z. SAl-Kamyani, K. Al-Shamsi and A. Ishtieh, *Constr Build Mater*., 2013, ***39***, 77–81.
5 N. Su. H. Y. Fang, Z. H. Chen and F. S. Liu, *Cement Concrete Res*., 2000, ***30***, 1773–1783.
6 S. Hwang, J. Lee, U. G. Hong, J. C. Jung, D. J. Koh, H. Lim, C. Byun and I. K. Song, *J. Ind. Eng. Chem.,* 2012, ***18***, 243–248.
7 M. R. Gonzalez, A. M. Pereyra, R. M. Torres Sánchez and E. I. Basaldella, *J Colloid Interf Sci.,* 2013, ***48***, 21–24.
8 N. Su, Z. H. Chen and H. Y. Fang, *Cem. Concr. Res*., 2001, ***23***, 111–118.
9 Y. S. Tseng, C. L. Huang and K. C. Hsu, *Cement Concrete Res.,* 2005, ***35***, 782–787.
10 S. I. Cho, K. S. Jung and S. I. Woo, *Appl. Catal., B* 2001, ***33***, 249–261.
11 V. A. Semikolenov, I. I. Ilyna and I. L. Simakova, *Appl. Catal., A Gen* 2001, ***211***, 91–107.
12 S. H. KO and T. C. Chou, *Ind. Eng. Chem. Res*., 1993, ***32***, 1579–1587.
13 S. H. KO, T. C. Chou and T. J. Yang, *Ind. Eng. Chem. Res*., 1995, ***34***, 457–467.
14 D. Chouchi, D. Gourgouillon, M. Courel, J. Vital and M. Nunes da Ponte, *Ind. Eng. Chem. Res*., 2001, ***40***, 2551–2554.
15 I. L. Simakova, Y. Solkina, I. Deliy, J. Warna and D. Y. Murzin, *Appl. Catal. A Gen* 2009, ***356***, 216–224.
16 I. I. Il'ina, I. L. Simakova and V. A. Semikolenov, *Kinet. Catal*., 2002, ***43***, 645–651.
17 M. S. Pavlin and N. J. Lawrenceville, US Patent 4310714, 1977.
18 M. M. Nair and H. Yen, F. Kleitz, *Comptes Rendus Chimie* 2014, ***17***, 641–655.
19 Z. H. Jia, Z. Y. Liu and Y. H. Zhao, *Chem. Eng. Technol.,* 2007*,* ***30,*** 1221–1227.
20 A. Alijani and A. Irankhah, *Chem. Eng. Technol*., 2013, ***36***, 552–558.
21 N. Gomes, Jose A. Teixeira and I. Belo, *Catal. Sci. Technol*., 2011, **1** , 86–92.

22 M. Jain, V. K. Garg and K. Kadirvelu, *Bioresour. Techno*l., 2011, ***102***, 600–605.

23 K. Zhong and Q. Wang, *Carbohydr. Polym*., 2010, ***80***, 19–25.

24 E. Senderov, I. Halasz and D. H. Olson, *Microporous Mesoporous Mater*., 2014, ***186***, 94–100.

25 R. Villa, C. Cristiani, G. Groppi, L. Lietti, P. Forzatti, U. Cornaro and S. Rossini, *J. Hazard. Mater.,* 2003, ***204–205***, 637–646.

26 F. Basile, L. Basini, M. D. Amore, G. Fornasari, A. Guarinoni, D. Matteuzzi, G. Del Piero, F. Trifirò and A. Vaccari, *J. Catal*., 1998, ***17***, 247–256.

27 C. P. Li and Y. W. Chen, *Thermochim. Acta* 1995, ***256***, 457–465.

28 M. Zarei, A. Niaei, D. Salari and A. Khataee, *J. Hazard. Mater*., 2010, ***173***, 544–551.

29 A. Hafizi, A. Ahmadpour, M. Koolivand-Salooki, M. M. Heravi and F. F. Bamoharram, *J. Ind. Eng. Chem.,* 2013, ***19***, 1981–1989.

A transformation of renewable biomass to useful chemicals, using waste fluid catalytic cracking catalyst supported nickel was accomplished.

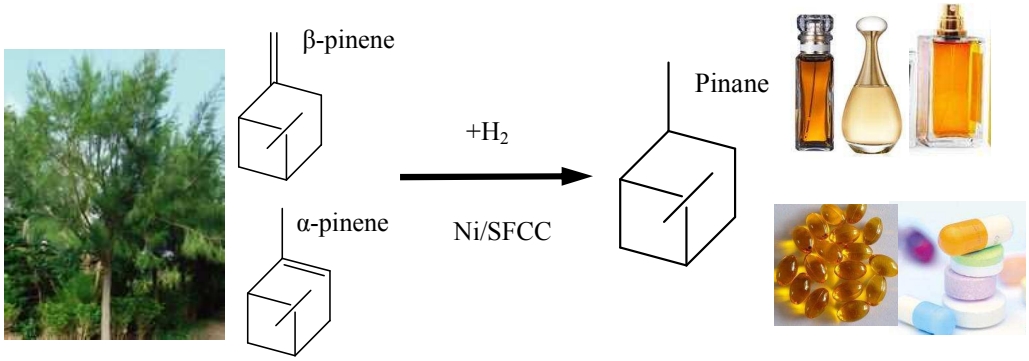

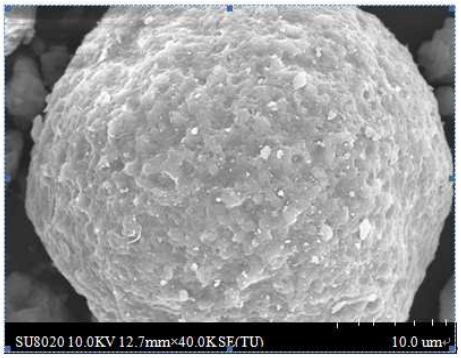

Fig. 1a

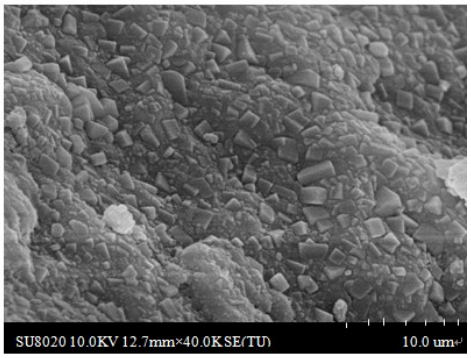

Fig.1b

Figure 1. SEM image of Ecat (a) and (b) NiO/Ecat.

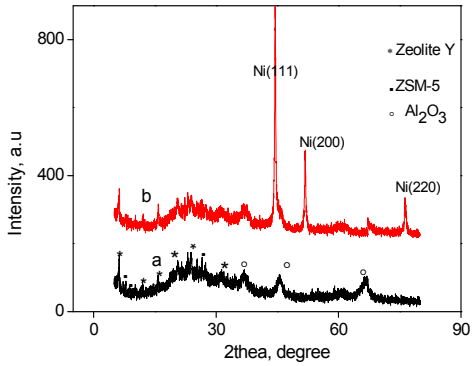

Figure 2. XRD spectra of Ecat (a) and (b) Ni/Ecat.

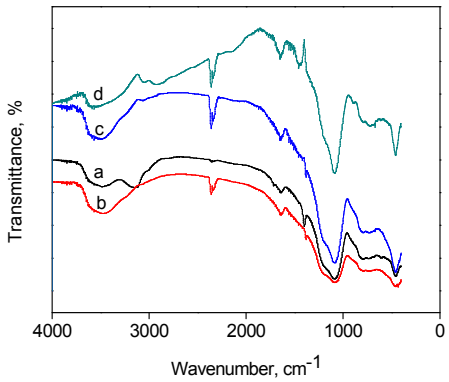

Figure 3. FTIR spectra of catalyst in various treatments (a) Ecat; (b) annealing Ecat; (c) NiO/Ecat; (d) Ni/Ecat.

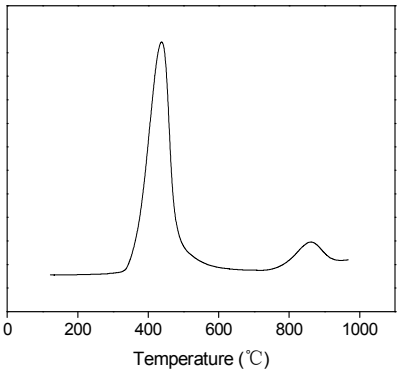

Figure 4. H_2-TPR of NiO/Ecat at 100-1000 °C.

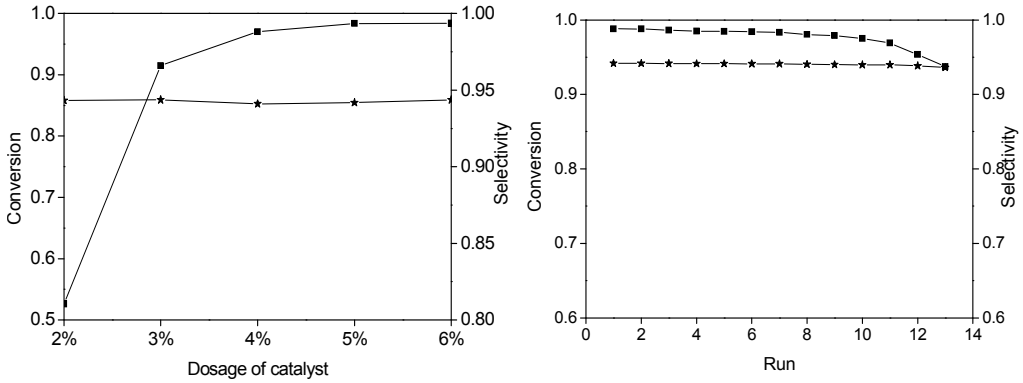

a b

Figure 5. Effect of the dosage of catalyst (a) and (b) Studies of catalyst reuse of Ni/Ecat. (■) represents the conversion of terebinth and (★) represents the selectivity of *cis*-pinane.

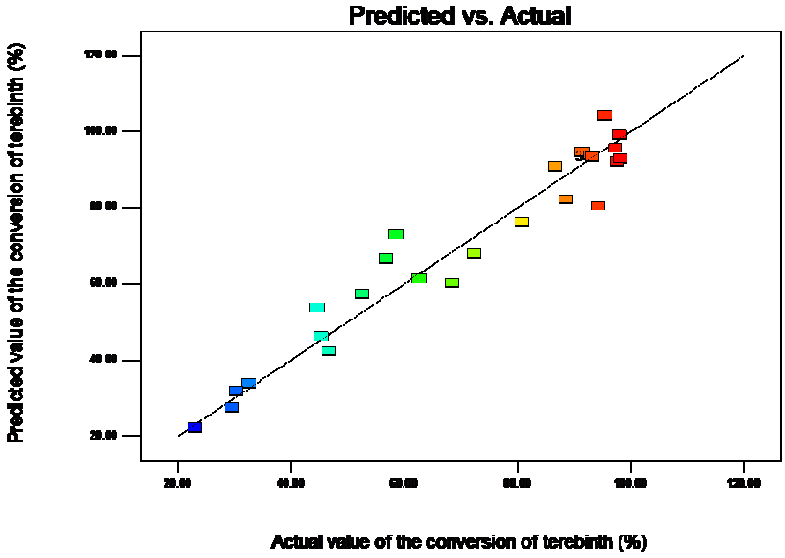

(a)

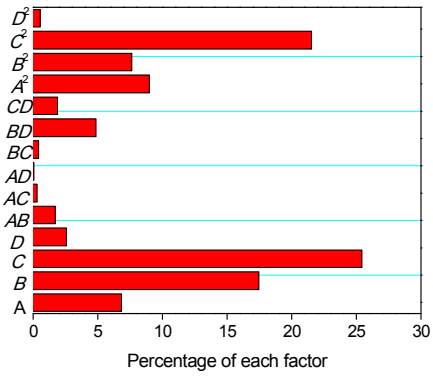

(b)

Figure 6. Predicted vs. actual values of conversion of terebinth (a) and pareto graphic analysis of the conversion of terebinth (b).

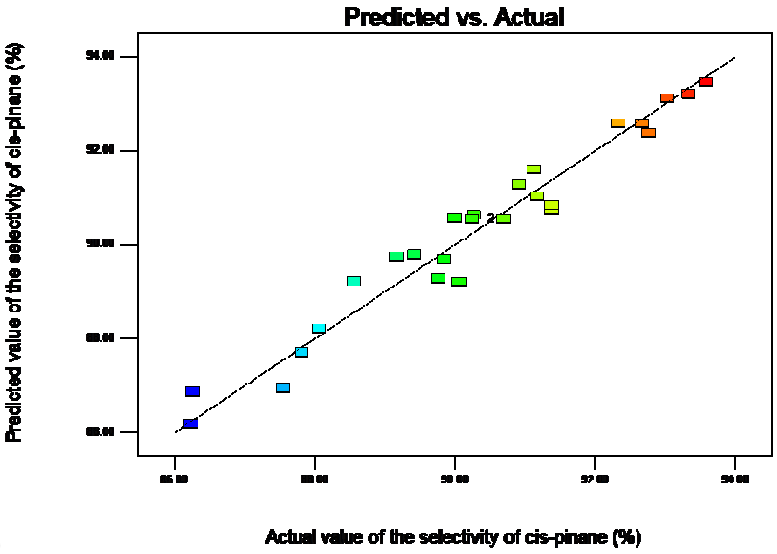

(a)

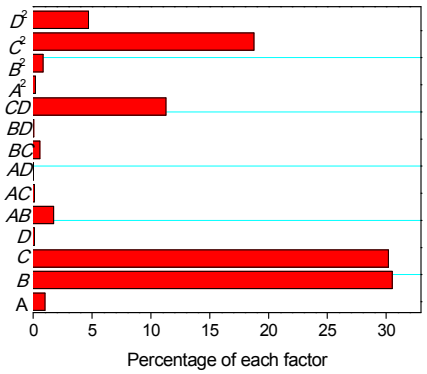

(b)

Figure 7. Predicted vs. actual values of the selectivity of *cis*-pinane (a) and pareto graphic analysis of the selectivity of *cis*-pinane (b).

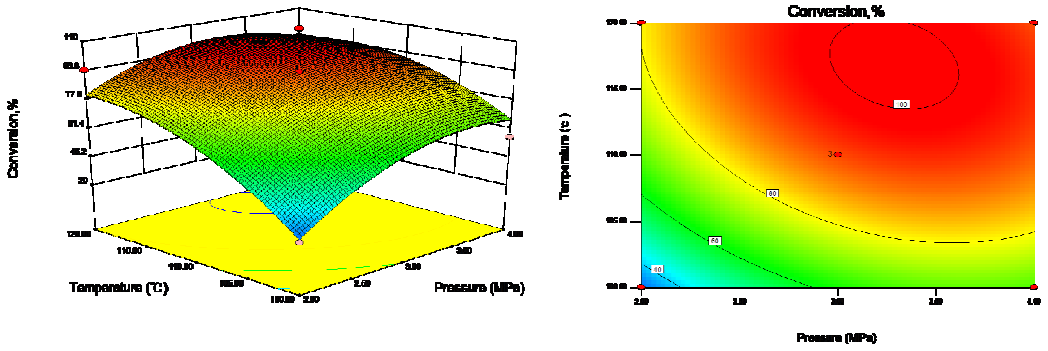

a

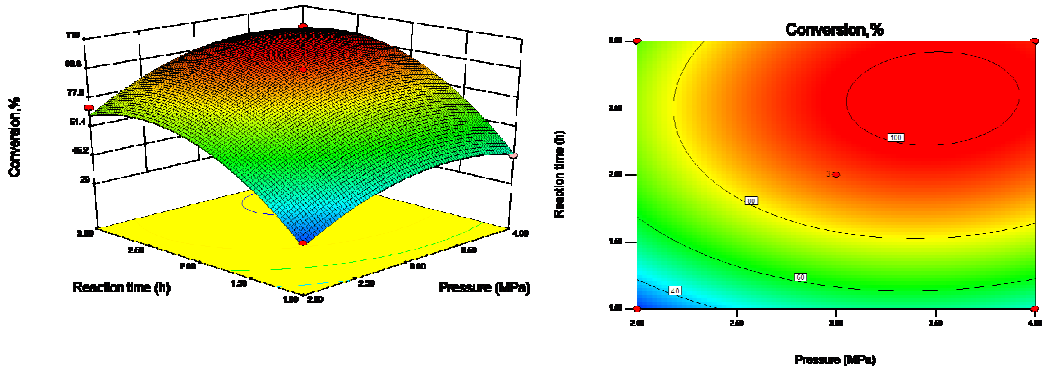

b

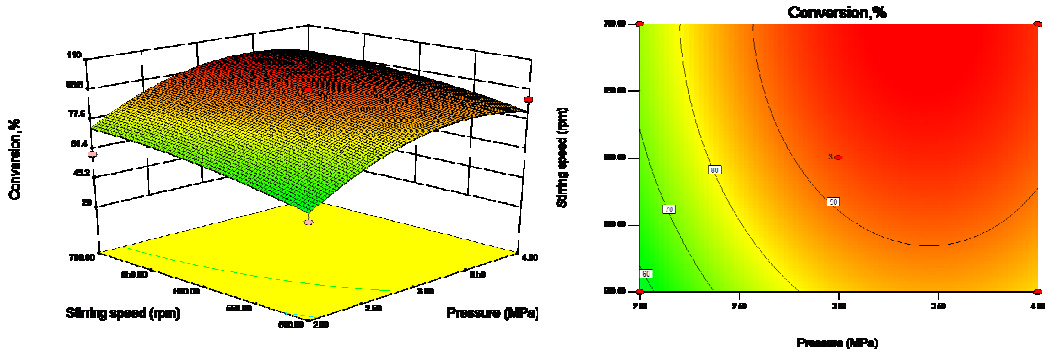

c

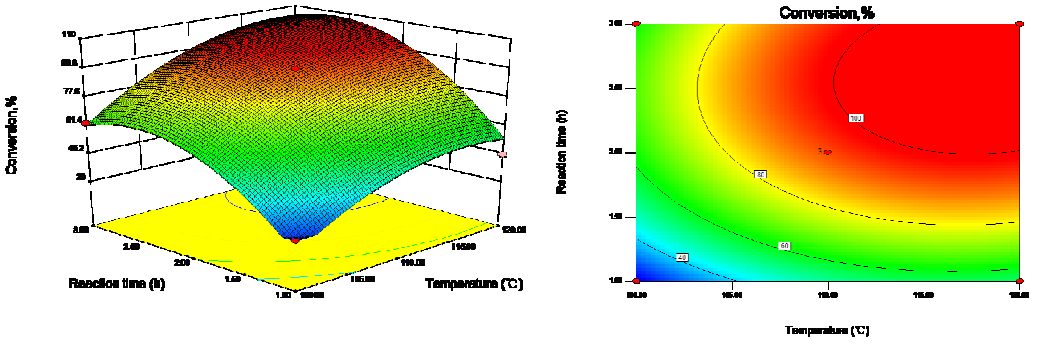

d

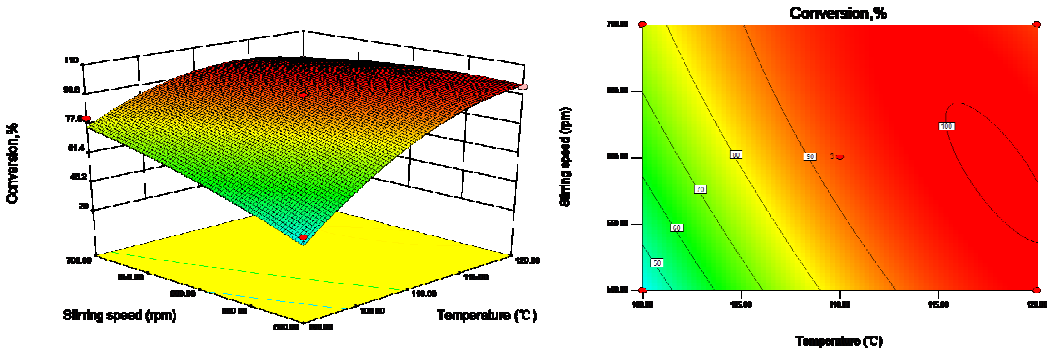

e

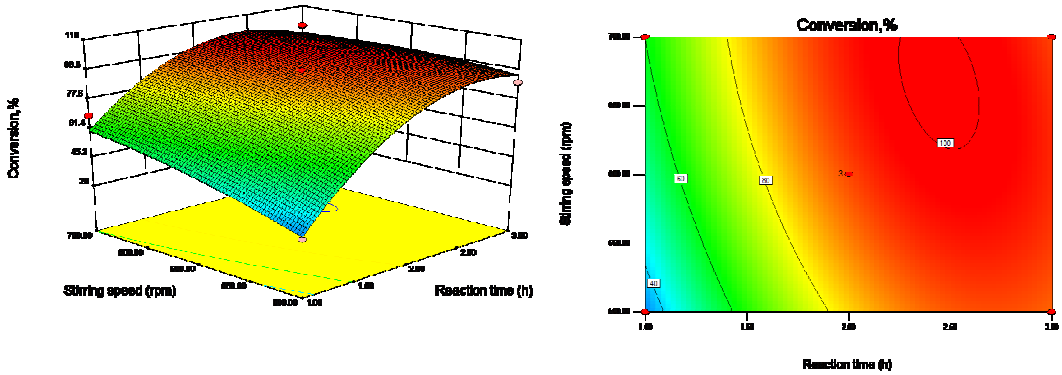

f

Figure 8. Effect of (a) temperature and pressure, (b) reaction time and pressure, (c) stirring speed and pressure, (d) reaction time and temperature, (e) stirring speed and temperature, (f) stirring speed and reaction time.

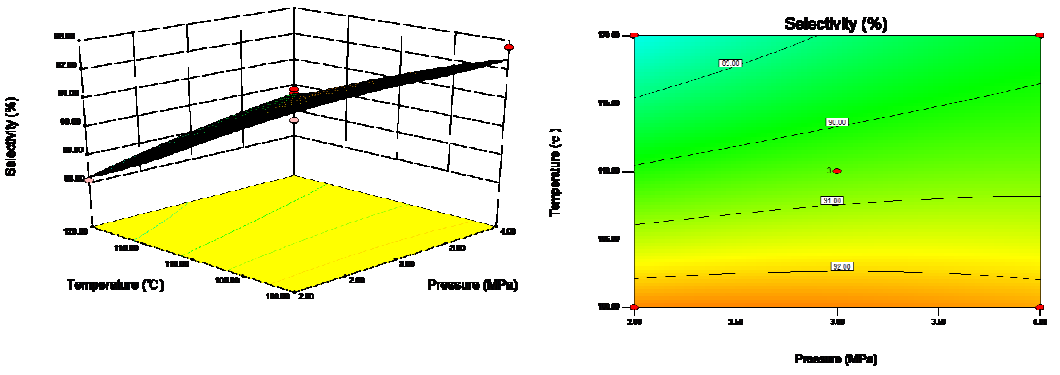

a

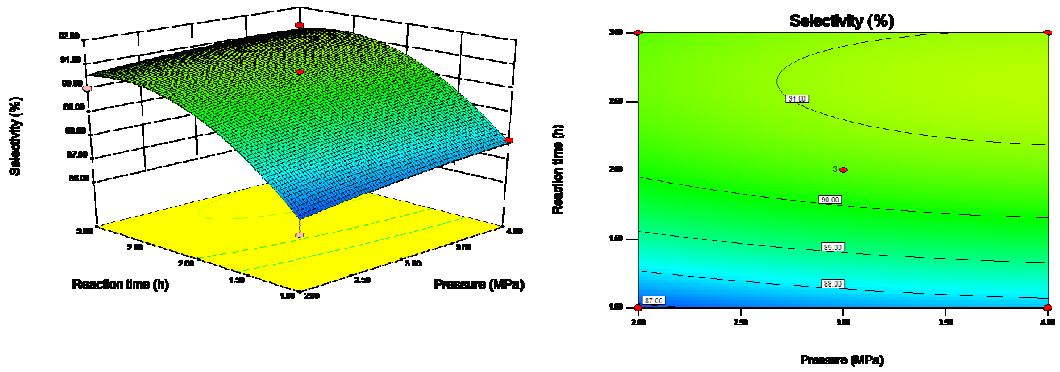

b

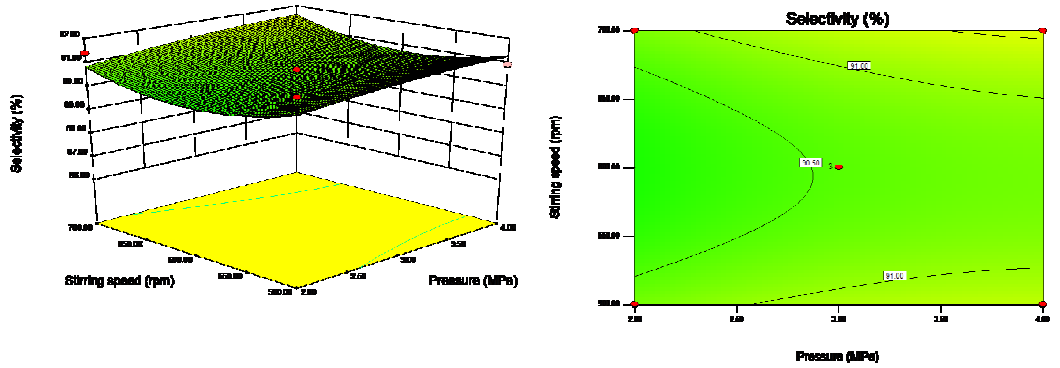

c

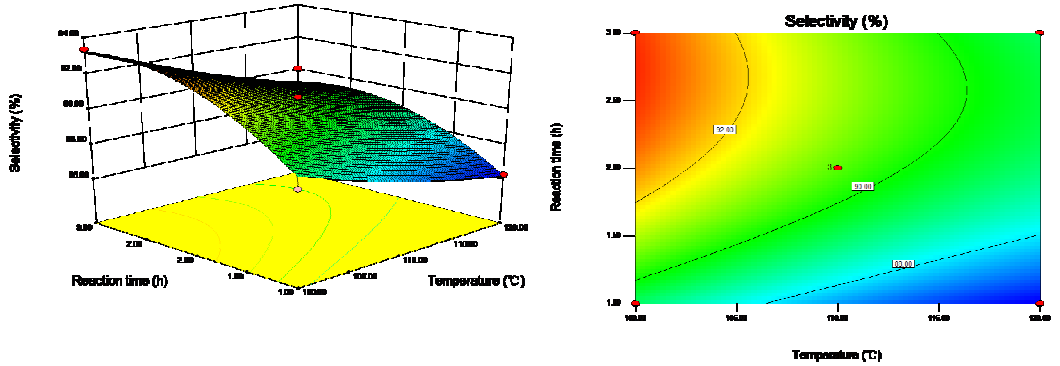

d

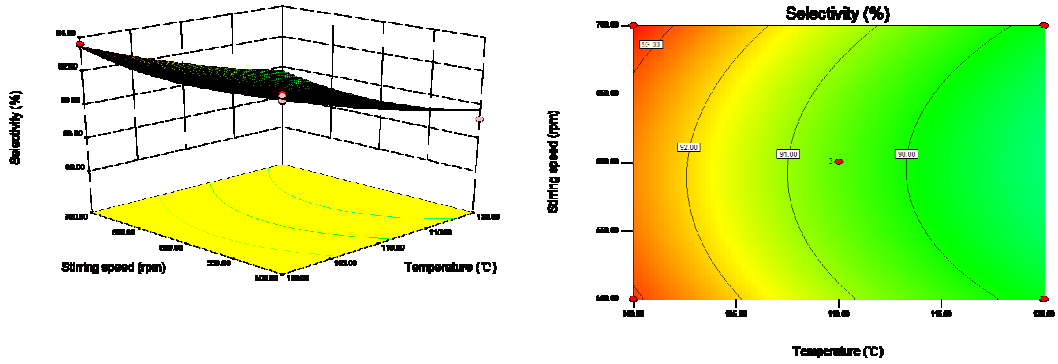

e

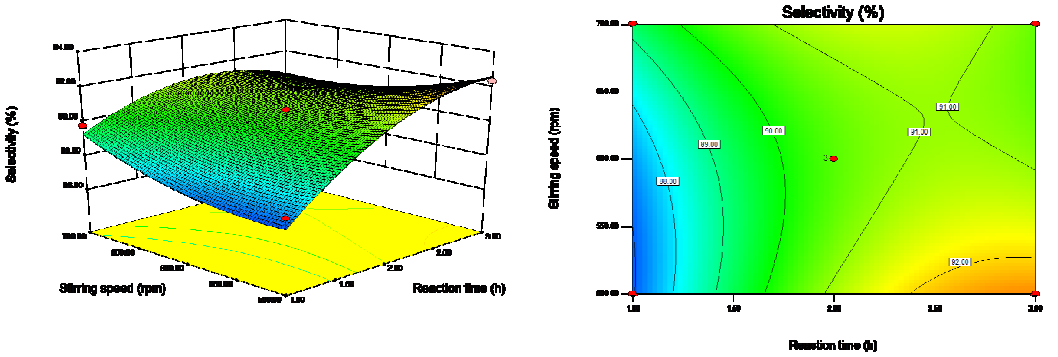

f

Figure 9. Effect of (a) temperature and pressure, (b) reaction time and pressure, (c) stirring speed and pressure, (d) reaction time and temperature, (e) stirring speed and temperature, (f) stirring speed and reaction time.

Table 1 Experimental ranges and levels of independent variables.

Variables	Coded variables	Ranges and levels		
		-1	0	1
Hydrogen pressure (MPa)	*A*	2	3	4
Temperature (℃)	*B*	100	110	120
Reaction time (h)	*C*	1	2	3
Stirring speed (rpm)	*D*	500	600	700

The Ni/Ecat dosage is 5% (accounted for terebinth).

Table 2 Fractional factorial central composite experimental design.

	Coded variable levels				%	%
Run	*A*	*B*	*C*	*D*	Y_1	Y_2
1	1	1	0	0	88.60	90.91
2	0	1	-1	0	56.82	92.76
3	1	-1	0	0	93.31	90.70
4	0	1	0	-1	30.33	92.67
5	0	0	0	0	68.48	89.78
6	1	0	0	-1	94.30	88.07
7	0	-1	0	1	95.55	90.06
8	-1	-1	0	0	93.31	90.24
9	0	1	0	1	44.70	86.24
10	1	0	0	1	32.64	87.55
11	-1	0	0	1	80.85	93.59
12	0	1	1	0	86.66	92.34
13	0	0	-1	1	29.65	86.26
14	0	0	1	-1	93.01	89.43
15	1	0	1	0	98.06	89.17
16	-1	0	-1	0	97.61	89.85
17	0	0	-1	-1	98.21	90.27
18	-1	0	1	0	46.73	93.03
19	1	0	-1	0	72.42	90.00
20	0	0	0	0	97.36	91.18
21	-1	1	0	0	45.35	87.82
22	0	0	0	0	22.98	88.56
23	0	-1	-1	0	91.45	91.13
24	-1	0	0	-1	58.60	91.39
25	0	0	1	1	62.60	93.33
26	0	-1	1	0	93.31	90.70
27	0	-1	0	-1	52.60	91.39

A, MPa hydrogen pressure; *B*, °C temperature; *C* h reaction time; *D*, rpm stirring speed, Y_1 observed conversion of terebinth; Y_2 observed selectivity of *cis*-pinane. The Ni/Ecat dosage is 5% (accounted for terebinth).

Table 3 Analysis of variance (ANOVA) of conversion (a) and selectivity (b) for selected model.

a

Source	Sum of squares	Degree of freedom	Mean square	*F*-value	*P*-value
Model	15971.15	14	1140.80	14.45	< 0.0001
A	1616.81	1	1616.81	20.48	0.0007
B	4141.11	1	4141.11	52.45	< 0.0001
C	6030.08	1	6030.08	76.37	< 0.0001
D	606.48	1	606.48	7.68	0.0169
AB	134.33	1	134.33	1.70	0.2166
AC	21.34	1	21.34	0.27	0.6126
AD	2.48	1	2.48	0.03	0.8623
BC	31.53	1	31.53	0.40	0.5393
BD	383.57	1	383.57	4.86	0.0478
CD	147.50	1	147.50	1.87	0.1967
A^2	948.21	1	948.21	12.01	0.0047
B^2	803.93	1	803.93	10.18	0.0078
C^2	2273.15	1	2273.15	28.79	0.0002
D^2	55.77	1	55.77	0.71	0.4171

A, MPa hydrogen pressure; *B*, °C temperature; *C* h reaction time; *D*, rpm stirring speed.

b

Source	Sum of squares	Degree of freedom	Mean square	*F*-value	*P*-value
Model	100.35	14	7.17	18.61	< 0.0001
A	1.26	1	1.26	3.26	0.0960
B	37.20	1	37.20	96.56	< 0.0001
C	36.67	1	36.67	95.17	< 0.0001
D	0.12	1	0.12	0.32	0.5849
AB	0.71	1	0.71	1.84	0.1995
AC	0.04	1	0.04	0.09	0.7682
AD	0.01	1	0.01	0.03	0.8588
BC	0.23	1	0.23	0.60	0.4542
BD	0.02	1	0.02	0.05	0.8187
CD	4.61	1	4.61	11.96	0.0047
A^2	0.09	1	0.09	0.22	0.6462
B^2	0.45	1	0.45	1.16	0.3031
C^2	10.17	1	10.17	26.41	0.0002
D^2	2.54	1	2.54	6.59	0.0247

A, MPa hydrogen pressure; *B*, °C temperature; *C* h reaction time; *D*, rpm stirring speed.

Table 4 Optimization results using response surface method.

	Optimal terebinth conversion (a)	Optimal *cis*-pinane selectivity (b)
Hydrogen pressure (MPa)	3.2	2.7
Temperature (°C)	110	101
Reaction time (h)	2.3	2.6
Stirring speed (rpm)	540	500

Table 5 Comparrsion between predicted and observed optimized values.

	Hydrogen pressure (MPa)	Temperature (°C)	Reaction time (h)	Stirring speed (rpm)	Predicted (%)		Observed (%)		% Error	
a	3.2	110	2.3	540	C	99.90	C	98.90	C	1.0
					S	90.97	S	94.00	S	3.3
b	2.7	101	2.6	500	C	53.80	C	52.40	C	2.6
					S	94.50	S	94.40	S	0.1

C, conversion of terebinth; S, selectivity of *cis*-pinane